We are IntechOpen, the world's leading publisher of Open Access books Built by scientists, for scientists

4,800
Open access books available

122,000
International authors and editors

135M
Downloads

Our authors are among the

154
Countries delivered to

TOP 1%
most cited scientists

12.2%
Contributors from top 500 universities

CLARIVATE ANALYTICS BOOK CITATION INDEX INDEXED

WEB OF SCIENCE™

Selection of our books indexed in the Book Citation Index in Web of Science™ Core Collection (BKCI)

Interested in publishing with us?
Contact book.department@intechopen.com

Numbers displayed above are based on latest data collected.
For more information visit www.intechopen.com

Chapter 7

X-ray Digital Tomosynthesis Imaging — Comparison of Reconstruction Algorithms in Terms of a Reduction in the Exposure Dose for Arthroplasty

Tsutomu Gomi

Additional information is available at the end of the chapter

http://dx.doi.org/10.5772/60920

Abstract

Aims The purpose of this review was (1) to identify indications for volumetric X-ray digital tomosynthesis by using a conventional reconstruction technique [the filtered back-projection (FBP) algorithm] and modern reconstruction techniques [the maximum likelihood expectation maximization (MLEM) and simultaneous iterative reconstruction techniques (SIRT)] and (2) to compare the conventional and modern reconstruction techniques in terms of a reduction in the exposure dose.

Review The methods included the following: (1) an overview and analysis of the characteristics of the FBP, MLEM, and SIRT algorithms; (2) an overview of the properties of phantom imaging for arthroplasty when imaging overlying structures and the effect of those properties on various artifacts in images; and (3) a review of each method regarding exposure reductions.

Summary In the phantom study, the MLEM and SIRT techniques can suppress streak artifacts; therefore, they warrant further evaluation in comparison with FBP. With the FBP technique, the exposure dose may be decreased to half of the reproducibility for a reconstructed prosthesis phantom image. The results show the characteristics of each technique that need to be considered in clinical practice (better suppression of streak artifacts: MLEM and SIRT; better reproducibility: FBP). In addition, understanding the advantages of each reconstruction technique during digital tomosynthesis imaging will improve diagnostic accuracy in clinical applications.

Keywords: Tomosynthesis, arthroplasty, exposure dose, reconstruction algorithm

1. Introduction

Digital tomosynthesis is a limited-angle image reconstruction method where a dataset of projections acquired at regular intervals during a single acquisition pass is used to reconstruct planar sections posteriori. Digital tomosynthesis also provides the additional benefits of digital imaging [1-17], as well as the tomographic benefits of computed tomography (CT) at decreased radiation doses and lower costs using an approach that can easily be implemented in conjunction with radiography. Digital tomosynthesis is a promising technique for improving early detection rates of cancer [6-7, 9-10, 13-14] because it can provide three-dimensional (3D) structural information by reconstructing an entire image volume from a sequence of projection-view radiograms acquired at a small number of projection angles over a limited angular range; the total radiation dose is comparable with that used during conventional radiography.

X-ray CT has continually matured, and it now constitutes a powerful tool in medical diagnostics. Metal artifacts influence image quality by reducing contrast and obscuring detail, thus impairing the detectability of structures of interest; in the worst case, this can make diagnosis impossible (Fig. 1).

Various digital tomosynthesis reconstruction methods have been explored previously [17]. Nevertheless, image quality assessments have been based on the use of phantoms with features that did not address radiation doses. In fact, to date, no studies have quantitatively compared digital tomosynthesis algorithms in terms of image quality and radiation doses. One recently developed CT technique, iterative reconstruction (IR), was found to effectively decrease quantum noise and radiation exposure [18]. IR may yield improvements in image quality and a reduction in the exposure dose in comparison with the conventional filtered back-projection (FBP) technique.

We chose to focus on the conventional FBP, statistical reconstruction technique [maximum likelihood expectation maximization (MLEM) [19]], and the algebraic reconstruction technique [simultaneous IR technique (SIRT) [20]]. We evaluated and compared the characteristics of the reconstructed images and the possible reduction in the radiation dose associated with FBP, MLEM, and SIRT algorithms for hip prosthesis phantoms. The algorithms were implemented using a digital tomosynthesis system and were experimentally evaluated by obtaining measurements using a phantom.

2. Tomosynthesis system

The tomosynthesis system (SonialVision Safire II, Shimadzu Co., Kyoto, Japan, Fig. 2) comprised an X-ray tube with a 0.4 mm focal spot and a 362.88 × 362.88 mm digital flat-panel detector composed of amorphous selenium. Each detector element was 150 × 150 μm in size. Tomography was performed linearly with a total acquisition time of 6.4 s {80 kVp, 250 mA, 20 ms/view, reference effective dose: 0.69 mSv [International Commission on Radiological Protection (ICRP) 103], half effective dose: 0.42 mSv (80 kVp, 250 mA, 14 ms/view), quarter

http://dx.doi.org/10.5772/60920

Figure 1. Comparison of metal artifact images with images obtained from each modality [CT (axial and coronal images) and conventional FBP tomosynthesis image].

effective dose: 0.24 mSv (80 kVp, 250 mA, 7 ms/view), and an acquisition angle of 40° (74 projections). The reconstructed images (0.272 mm/pixel) were obtained at 1 mm reconstruction intervals. (Table 1, Fig. 3)

Tomosynthesis system	**SonialVision Safire II (Shimadzu Co., Japan)**
X-ray focal spot	0.4 mm
Detector area	362.88 × 362.88 mm
Detector type	Direct conversion-type flat-panel detector (amorphous selenium)
Detector element	150 × 150 μm
X-ray tube voltage	80 kVp
X-ray tube current	250 mA
Acquisition time	Reference dose: 20 ms/view
	Half dose: 14 ms/view
	Quarter dose: 7 ms/view
Acquisition angle	40°
Projections	74
Reconstruction interval	1 mm

Table 1. The detailed estimates of the acquisition parameters.

3. Phantom specifications

A hip prosthesis phantom (PerFix HA CMT91006; Japan Medical Materials Co., Tokyo, Japan; Fig. 4) was used in a polymethyl methacrylate (PMMA) case filled with water (case φ, 200 × 300 mm). The prosthetic phantom were designed to evaluate image reconstruction quality for in-plane (x-y plane) and out-plane (z-axis) images.

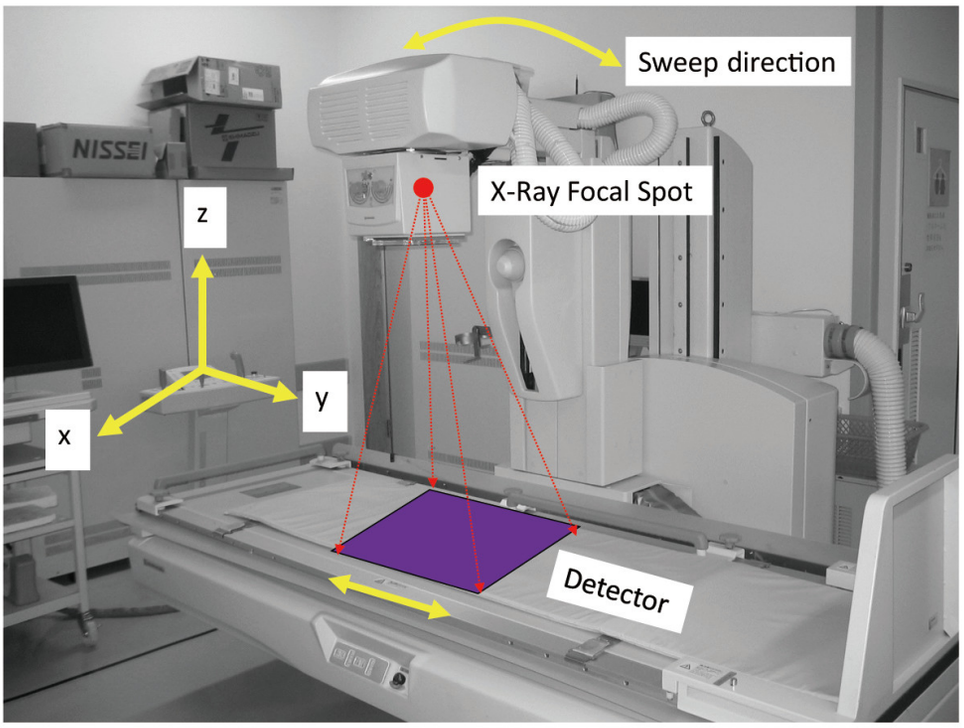

Figure 2. Illustration of a SonialVision Safire II tomosynthesis system (Shimadzu Co., Kyoto, Japan). This system acquires 3D projection data by linear motion in the y-axis direction. The detector uses a direct conversion-type flat-panel detector (FPD).

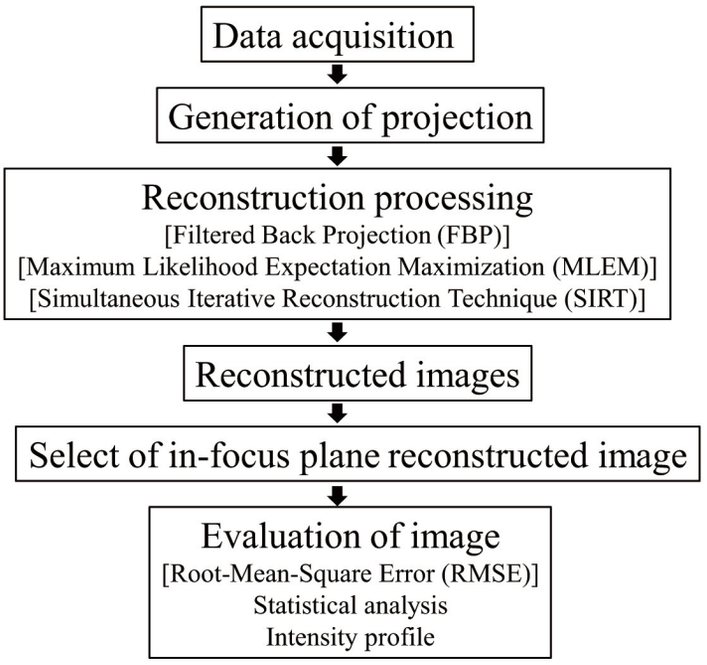

Figure 3. Flow chart of image reconstruction processing and image evaluation.

http://dx.doi.org/10.5772/60920

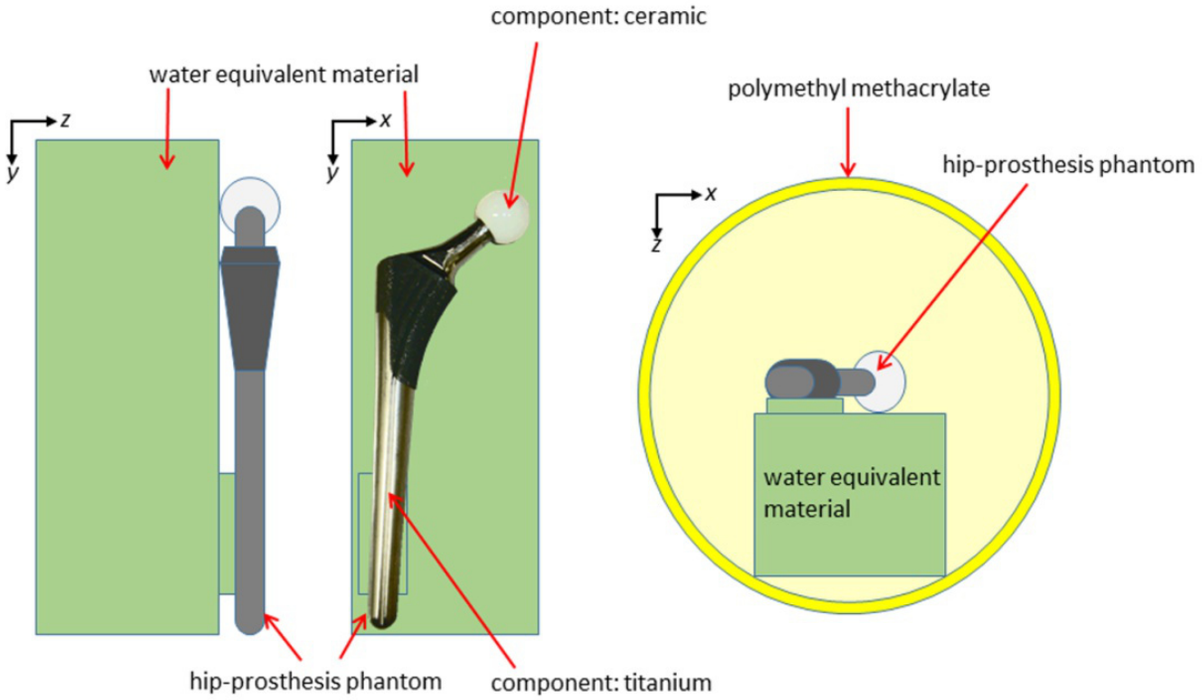

Figure 4. Illustration of the hip-prosthesis phantom used in this study.

4. Image reconstruction for digital tomosynthesis

In FBP algorithms, which are widely used in tomography, many projections are acquired for cross-sectional image reconstruction. The relationship between the radon transform and cone-beam projections has been thoroughly studied, and cone-beam reconstruction solutions have been obtained previously [14]. Two-dimensional (2D) image filtering via multiplication of the Fourier transform by means of a Ramp or Shepp-Logan (SL) filter kernel restores the proper impulse shape for the reconstructed image. The FBP algorithm generally provides highly precise 3D reconstruction images [14]. In this study, a conventional SL filter kernel was used to reconstruct FBP images (Fig. 5).

IR algorithms perform reconstruction recursively [21-22], unlike the one-step operation used in back projection and FBP algorithms. Instead, reconstruction is accomplished by iteratively updating unknown linear attenuation coefficients by minimizing the error between the measured and calculated projection data.

The original method in this family of algebraic reconstruction techniques (ARTs) [20] has already been determined. ART features fast convergence speed because only a single projection value is used to update linear attenuation coefficients at a given time point, but it converges to a least-squares solution that can result in considerable noise when severely ill-posed inverse problems, such as limited-angle reconstruction, are being solved. Variations have been

proposed regarding ART implementation for facilitating improvements. ART can be modified according to other methods such as SIRT [20], depending on the amount of projection data and the method used to update the current estimation (Fig. 6).

On the other hand, MLEM methods consisting of two steps per iteration (in which the tomosynthesis acquisition process is modeled in a forward step and the reconstructed object is updated in a backward step) have also been proposed for digital tomosynthesis. The most commonly studied method in digital tomosynthesis is MLEM introduced for digital tomosynthesis by Wu et al. [19]. MLEM and SIRT are applied iteratively such that the reconstructed volume projections, which are computed using an image formation model, resemble the experimental projections (Figs. 6-7). In this chapter, seventeen MLEM and SIRT iterations were used to improve image quality (to attain highest contrast and to minimize metal artifacts). The FBP, MLEM, and SIRT image reconstruction calculations from real projection data of a digital tomosynthesis system were performed using MATLAB (Mathworks, Natick, MA, USA).

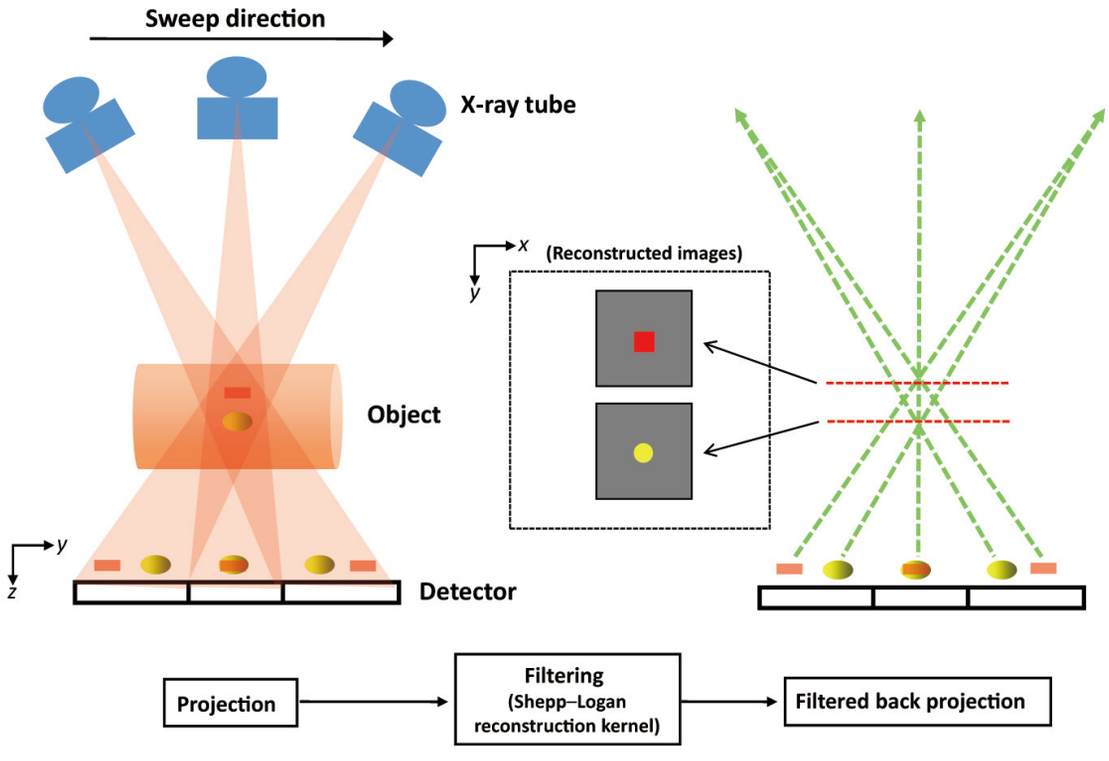

Figure 5. Concept of the FBP-processing method for tomosynthesis.

5. Evaluation

In the chapter, the metal artifact-reduction and image quality performance was evaluated using the intensity profile and root-mean-square error (RMSE). The intensity profiles were

http://dx.doi.org/10.5772/60920

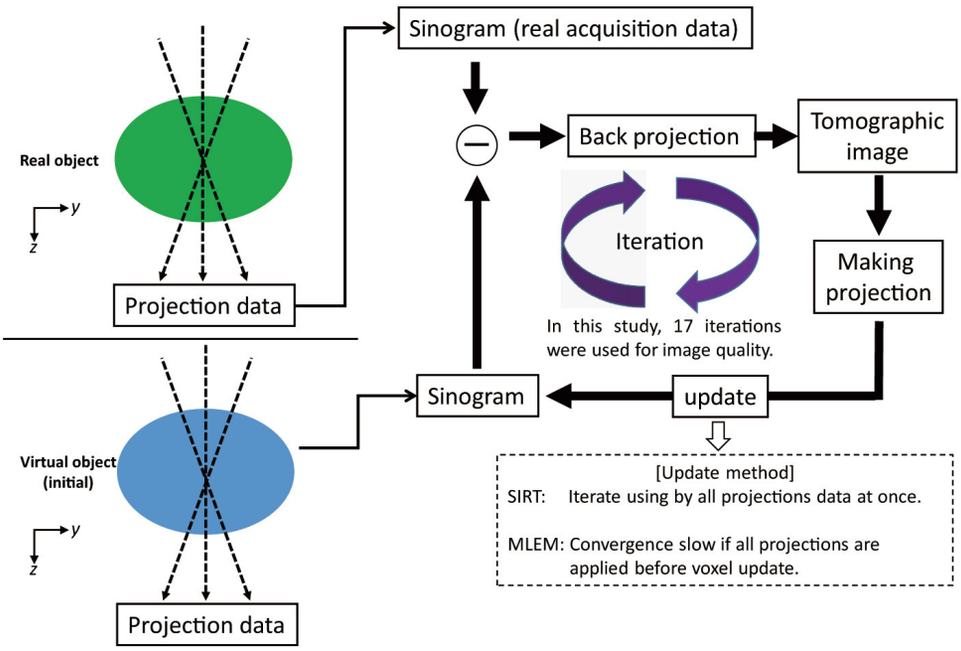

Figure 6. Concept of the IR-processing method (MLEM and SIRT) for tomosynthesis.

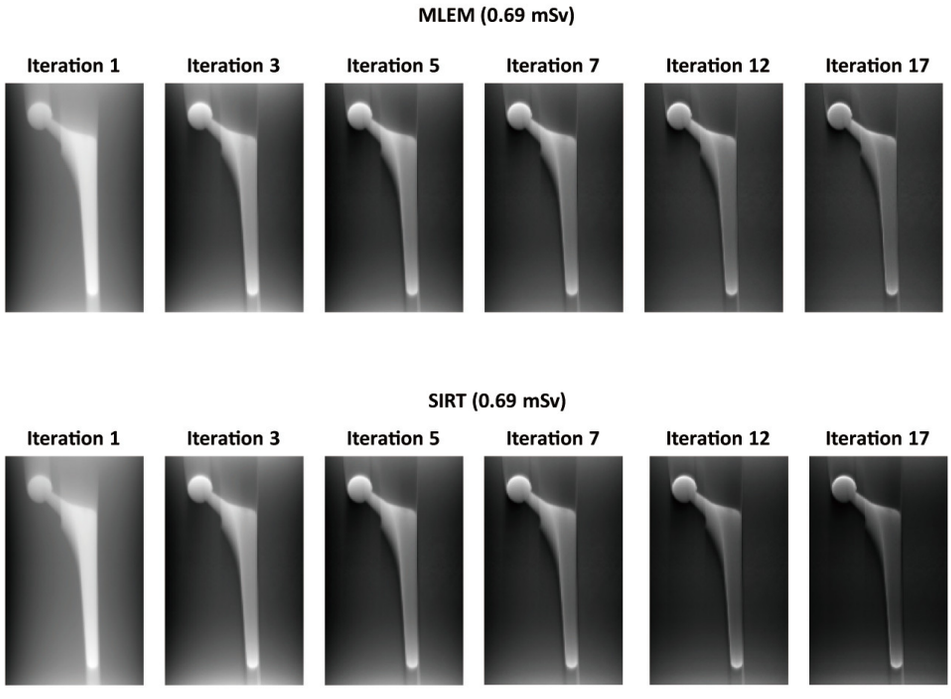

Figure 7. Comparison between tomosynthesis images (different iteration) and those obtained from the imaging algorithms of MLEM and SIRT technique in the in-focus plane. The MLEM and SIRT tomosynthesis images for the corresponding prosthesis phantom are displayed with the same window width and window level. The x-ray source moved in the vertical direction relative to the image shown. Image quality (reproducibility and artifact) is improved by increasing the number of iterations.

compared using different reconstruction methods in the in-focus plane. Another important metric to be considered is RMSE, which can be computed by obtaining the root of the summation of the square of the standard deviation and the square of the bias. The errors in the image plane are defined in terms of RMSE as

$$RMSE = \sqrt{\sum_{i=1}^{n} \left(X - x_i\right)^2 / n} \quad (1)$$

where X is the observed image, $x_i$is the referenced image, and n is the number of compounds in the analyzed set.

The effects of image artifacts and quality were assessed in paired *t*-test. Statistical tests were used to assess differences between pixel values (from intensity profile) of FBP, MLEM, and SIRT. We performed the tests on a total of 84 samples. The statistical analysis was performed in SPSS for Windows, version 21.0 (SPSS Inc., Chicago, IL, USA). All probability (*P*) values <0.05 were assumed to denote statistical significance.

6. Results

A comparison of the intensity profiles and RMSEs of the tomosynthesis images revealed that tomosynthesis (IR algorithm) decreased the number of metal and beam hardening artifacts in the reconstructed images. Furthermore, this IR technique can reduce quantum noise, and the noise structure was slightly smoother. The MLEM and SIRT techniques can suppress streak artifacts; therefore, they warrant further evaluation in comparison with FBP (Figs. 8-10).

The comparison of the reference exposure dose (0.69 mSv for the FBP image) with the reduced exposure dose (0.42 mSv for the FBP image) involved the paired *t*-test: p = 0.112 (not a statistically significant difference), t = −1.664, degrees of freedom (DF) = 20, 95% confidence interval (CI): −0.120 to 0.013. The comparison of the reference exposure dose (0.69 mSv for the MLEM image) and the reduced exposure dose (0.42 mSv for the MLEM image) was also based on the paired *t*-test: p < 0.05 (statistically significant difference), t = −7.386, DF = 20, 95% CI: -0.108 to -0.060. The comparison of the reference exposure dose (0.69 mSv for the SIRT image) with the reduced exposure dose (0.42 mSv for the SIRT image) involved the paired *t*-test: p < 0.05 (statistically significant difference), t = −7.372, DF = 20, 95% CI: −0.126 to −0.070. With the FBP technique, it was possible to maybe maintain the reproducibility of a reconstructed image with an approximately 50% reduction in the radiation dose. The results show the characteristics of each technique that need to be considered in clinical practice (better suppression of streak artifacts: MLEM and SIRT; better reproducibility: FBP).

http://dx.doi.org/10.5772/60920

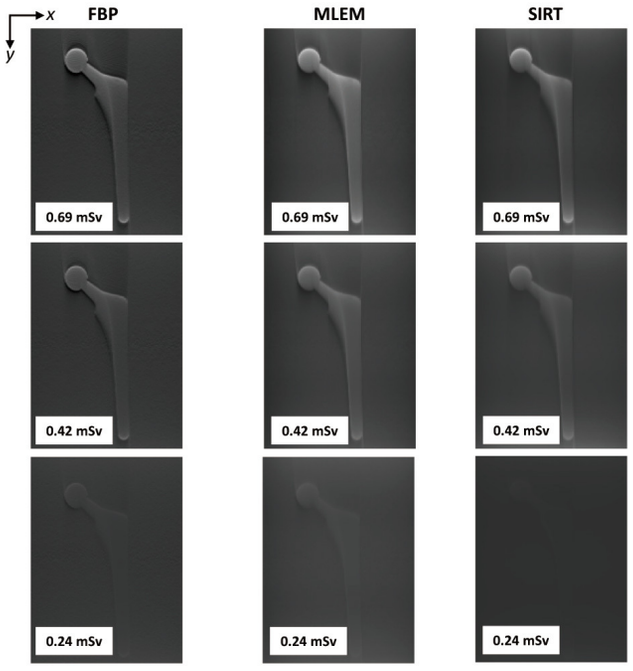

Figure 8. Comparison between tomosynthesis images (different reconstruction technique and different exposure dose, FBP filter kernel: Shepp-Logan, IR iteration: 17) and those obtained from the imaging algorithms of FBP, MLEM, and SIRT techniques in the in-focus plane. The FBP, MLEM, and SIRT tomosynthesis images for the corresponding prosthesis phantom are displayed with the same window width and window level. The x-ray source moved in the vertical direction relative to the image shown.

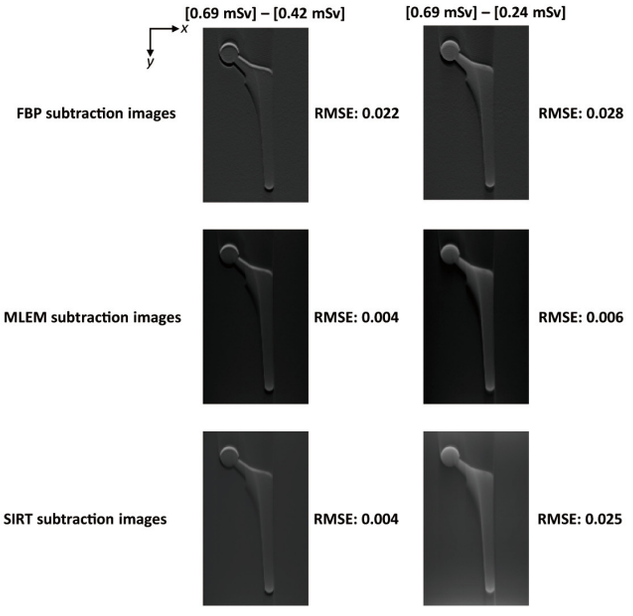

Figure 9. Comparison between tomosynthesis subtraction images (FBP filter kernel: Shepp-Logan, IR iteration: 17) and those obtained from the imaging algorithms of FBP, MLEM, and SIRT techniques in the in-focus plane. The FBP, MLEM, and SIRT tomosynthesis images for the corresponding prosthesis phantom are displayed with the same window width and window level. The x-ray source moved in the vertical direction relative to the image shown.

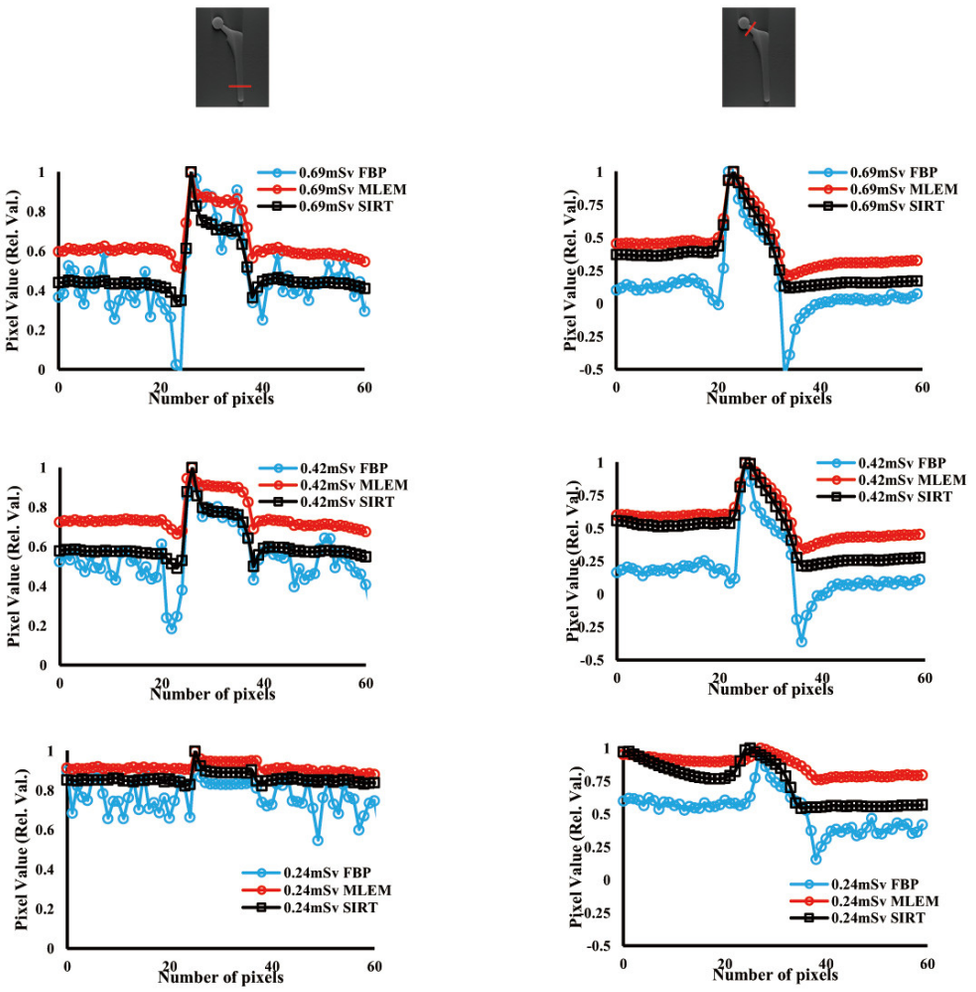

Figure 10. Comparison between intensity profiles using tomosynthesis (different exposure dose) in the in-focus plane. Artifacts (part of undershooting) are reduced by the IR technique for tomosynthesis.

7. Conclusion

In this study, the results of a prosthesis phantom study suggest that digital tomosynthesis (IR algorithm) can produce improved image quality compared with that by conventional FBP tomosynthesis by the same exposure dose level. In addition, the IR algorithm apparently facilitates the significant improvement of images corrupted by metal artifacts.

With the FBP technique, the exposure dose may be decreased to half of the reproducibility for a reconstructed prosthesis phantom image.

In addition, understanding the advantages of each reconstruction technique during digital tomosynthesis imaging (better suppression of streak artifacts: IR algorithm; better reproducibility: FBP) will improve diagnostic accuracy in clinical applications.

http://dx.doi.org/10.5772/60920

Author details

Tsutomu Gomi

Address all correspondence to: gomi@kitasato-u.ac.jp

School of Allied Health Sciences, Kitasato University, Japan

References

[1] Ziedses des, Plante BG. Eine neue methode zur differenzierung in der roentgenographie (planigraphie). Acta radiologica 1932; 13 182-192.

[2] Miller ER, McCurry EM, Hruska B. An infinite number of laminagrams from a finite number of radiographs. Radiology 1971; 98 249-255.

[3] Grant DG. Tomosynthesis. A three-dimensional radiographic imaging technique. IEEE transactions on bio-medical engineering 1972; 19 20-28.

[4] Baily NA, Lasser EC, Crepeau RL. Electrofluoro-plangigraphy. Radiology 1973; 107 669-671.

[5] Kruger RA, Nelson JA, Ghosh-Roy D, Miller FJ, Anderson RE, Liu PY. Dynamic tomographic digital subtraction angiography using temporal filteration. Radiology 1983; 147 863-867.

[6] Sone S, Kasuga T, Sakai S, Aoki J, Izuno I, Tanizaki Y, Shigeta H, Shibata K. Development of a high-resolution digital tomosynthesis system and its clinical application. Radiographics 1991; 11 807-822.

[7] Sone S, Kasuga T, Sakai F, Kawai T, Oguchi K, Hirano H, Li F, Kudo K, Honda T, Hanouda M. Image processing in the digital tomosynthesis for pulmonary imaging. European Radiology 1995; 5 96-101.

[8] Machida H, Yuhara T, Mori T, Ueno E, Moribe Y, Sabol JM. Optimizing parameters for flat-panel detector digital tomosynthesis. Radiographics 2010; 30 549-562.

[9] Vikgren J, Zachrisson S, Svalkvist A, Johnsson AA, Boijsen M, Flinck A, Kheddache S, Båth M. Comparison of chest tomosynthesis and chest radiography for detection of pulmonary nodules: Human observer study of clinical cases. Radiology 2008; 217 251-256.

[10] Skaane P, Bandos AI, Gullien R, Eben EB, Ekseth U, Haakenaasen U, Izadi M, Jebsen IN, Jahr G, Krager M, Niklason LT, Hofvind S, Gur D. Comparison of digital mammography alone and digital mammography plus tomosynthesis in a population-based screening program. Radiology 2013; 267 47-56.

[11] Stiel G, Stiel LG, Klotz E, Nienaber CA. Digital flashing tomosynthesis: A promising technique for angiographic screening. IEEE transactions on medical imaging 1993; 12 314-321.

[12] Duryea J, Dobbins JT, Lynch JA. Digital tomosynthesis of hand joints for arthritis assessment. Medical Physics 2003; 30 325-33.

[13] Niklason LT, Christian BT, Niklason LE, Kopans DB, Castleberry DE, Opsahl-Ong BH, Landberg CE, Slanetz PJ, Giardino AA, Moore R, Albagli D, DeJule MC, Fitzgerald PF, Fobare DF, Giambattista BW, Kwasnick RF, Liu J, Lubowski SJ, Possin GE, Richotte JF, Wei CY, Wirth RF. Digital tomosynthesis in breast imaging. Radiology 1997; 205 399-406.

[14] Dobbins JT III, Godfrey DJ. Digital x-ray tomosynthesis: Current state of the art and clinical potential. Physics in medicine and biology 2003; 48 R65-106.

[15] Gomi T, Hirano H. Clinical potential of digital linear tomosynthesis imaging of total joint arthroplasty. Journal of Digital Imaging 2008; 21 312-322.

[16] Gomi T, Hirano H, Umeda T. Evaluation of the x-ray digital linear tomosynthesis reconstruction processing method for metal artifact reduction. Computerized Medical Imaging and Graphics 2009; 33 257-274.

[17] Gomi T, Hirano H, Nakajima M. Recent advance in arthroplasty. In: X-ray digital linear tomosynthesis imaging of arhtoroplasty. Rijeka: InTech 2012; 95-108.

[18] Marin D, Nelson RC, Schindera ST, Richard S, Youngblood RS, Yoshizumi TT, Samei E. Low-tube-voltage, high-tube-current multidetector abdominal CT: Improved image quality and decreased radiation dose with adaptive statistical iterative reconstruction algorithm-initial clinical experience. Radiology 2010; 254 145-153.

[19] Wu T, Stewart A, Stanton M, McCauley T, Phillips W, Kopans DB, Moore RH, Eberhard JW, Opsahl-Ong B, Niklason L, Williams MB. Tomographic mammography using a limited number of low-dose cone-beam projection images. Medical Physics 2003; 30 365-380.

[20] Gordon R, Bender R, Hermen GT. Algebraic reconstruction techniques (ART) for three-dimensional electron microscopy and x-ray photography. Journal of theoretical biology 1970; 29 471-481.

[21] Bleuet P, Guillemaud R, Magnin I, Desbat L. An adapted fan volume sampling scheme for 3D algebraic reconstruction in linear tomosynthesis. IEEE Trans Nucl Sci 2001; 3 1720-1724.

[22] Wu T, Zhang J, Moore R, Rafferty E, Kopans D, Meleis W, Kaeli D. Digital tomosynthesis mammography using a parallel maximum-likelihood reconstruction method. Proc SPIE 2004; 5368 1-11.